Materials and Design 189 (2020) 108499

Contents lists available at ScienceDirect

Materials and Design

journal homepage: www.elsevier.com/locate/matdes

Thermally activated deformation mechanisms and solid solution softening in W-Re alloys investigated via high temperature nanoindentation

Johann Kappacher[a], Alexander Leitner[a], Daniel Kiener[b], Helmut Clemens[a], Verena Maier-Kiener[a,*]

[a]Department of Materials Science, Chair of Physical Metallurgy & Metallic Materials, Montanuniversität Leoben, Franz Josef-Str. 18, A-8700 Leoben, Austria
[b]Department of Materials Science, Chair of Materials Physics, Montanuniversität Leoben, Franz Josef-Str. 18, A-8700 Leoben, Austria

HIGHLIGHTS

- Constant indentation strain rate and jump tests were performed up to 800 °C.
- Temperature- and strain rate-sensitivity below 0.2 Tm are strongly decreased by Re.
- Reduced Peierls potential manifests as an increased activation volume below 400 °C.
- Activation energy is reduced by Re at low temperatures and not affected > 400 °C.

GRAPHICAL ABSTRACT

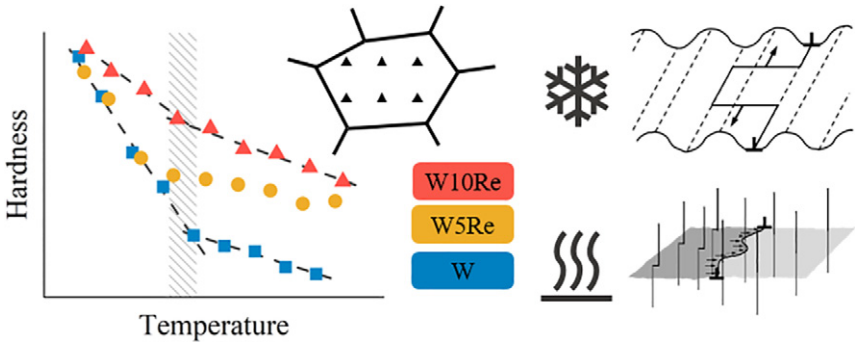

ARTICLE INFO

Article history:
Received 25 October 2019
Received in revised form 18 December 2019
Accepted 13 January 2020
Available online 18 January 2020

Keywords:
Refractory metals
High temperature deformation
Plastic deformation
Strain rate sensitivity

ABSTRACT

Thermally activated deformation mechanisms in three different W-Re alloys were investigated by performing high temperature nanoindentation experiments up to 800 °C. With increasing Re content the athermal hardness increases, while the temperature-dependent thermal contribution is strongly decreased. This results in a reduced strain rate sensitivity for W-Re alloys compared to pure W. The origin of this effect is a reduction of the Peierls potential due to Re, manifesting in an increased activation volume at lower temperatures. This gives rise to a solid solution softening effect, while at high-temperature application the mechanical behavior is governed by dislocation-dislocation interaction and solution strengthening.

1. Introduction

Tungsten, the metal with the highest melting point T_m of 3422 °C, and its alloys are extensively used for high-temperature applications [1-3]. The most outstanding temperature-related characteristic of W in particular, and body-centered cubic (*bcc*) metals in general, is the drastic decrease in flow stress with increasing temperature [4, 5]. This is owed to the non-planar core structure of the 1/2⟨111⟩ screw dislocations, resulting in a high lattice resistance for slip [6, 7]. Thus, the shear stress for plastic deformation at low temperatures is high compared to face-centered cubic (*fcc*) metals. This phenomenon is commonly attributed to the Peierls stress and diminishes at temperatures above ~0.2 T_m due to thermal activation of kink-pairs that migrate easily along the screw dislocation line [8, 9]. That part is therefore designated as thermal contribution to the flow stress and is responsible for the pronounced rate-dependent deformation

* Corresponding author.
E-mail address: verena.maier-kiener@unileoben.ac.at (V. Maier-Kiener).

https://doi.org/10.1016/j.matdes.2020.108499

behavior of W at room temperature (RT). Above ~0.2 T_m screw and edge dislocations exhibit a similar mobility. This temperature regime is thus referred to as athermal, meaning that no additional thermal activation is required for deformation [4, 5].

Although its high melting point makes W a promising candidate for high-temperature applications, it has some major drawbacks. Due to its high brittle to ductile transition temperature it has a low fracture toughness, low elongation to failure and generally a low formability at ambient temperature [8]. To face these issues, alloying with Re was developed, as this causes a ductilization effect [6,10-12]. Because the rarity of Re renders it a very expensive metal, W-Re alloys are not used extensively on a large scale. The most common applications nowadays are as thermocouples or focal tracks of anodes for X-ray tubes [13]. For the development of plasma-facing components in fusion reactors it is furthermore necessary to understand the effect of Re in W [14-18].

Experimental evidence that Re decreases the Peierls potential in W was found in the late 60s [19]. More recently, Romaner et al. [6] proved the concept that alloying with Re changes the properties of the 1/2⟨111⟩ screw dislocation from a symmetric to an asymmetric core and hence leads to a reduction in Peierls stress. The origin of this intrinsic effect stems from filling of the *d* band, resulting in a modification of the intermetallic bonding. It is known for almost half a century that solid solution softening occurs in group VI elements when alloying with elements from group V to VIII [11]. The effect is strongly temperature dependent and disappears at temperatures above ~0.2 T_m [11, 20]. Also, the solute content where the minimum hardness is reached depends strongly on the number of *s* and *d* electrons of the alloying element, leading to a highest solute content at the hardness-minimum for Re and lowest for Ni. At RT, a minimum in hardness is observed around 5% Re, which decreases with increasing temperature [20-23].

To experimentally study such effects in small volumes without the need for large quantities of expensive alloys, nanoindentation is the method of choice. Hardness and Young's modulus of a material can be investigated at high accuracy and reproducibility [24]. With increasing popularity of this technique, advanced testing protocols became available [25], allowing to determine the strain rate sensitivity and activation volume of plastic deformation processes [26,27]. These methods, combined with the possibility to test at elevated temperatures [28-31], provide a powerful tool to study thermally activated mechanisms for a better understanding of material behavior at higher temperatures.

2. Materials and methods

Three different alloy compositions were tested in this study, namely commercially pure W, W5Re and W10Re (in wt%). All samples were provided by Plansee SE (Reutte, Austria). The initial coarse-grained microstructure resulted from a solution heat treatment at 1700° for 2 h. Light optical micrographs, including the average grain size are shown in Fig. 1. Additional Vickers hardness (HV10) measurements were performed on an Emco-Test M4C025G3M.

Nanoindentation experiments were conducted on an InSEM-HT (Nanomechanics Inc., KLA, Oak Ridge, TN) with a continuous stiffness measurement unit. The frequency of the superimposed force signal was 100 Hz with a displacement amplitude of 2 nm. The system is mounted in a Tescan Vega3 scanning electron microscope (Tescan, Brno, Czech Republic) under high vacuum ($< 5.0 \times 10^{-4}$ mbar) to prevent sample surface degradation or oxidation of the indenter at elevated temperatures [28]. A tungsten carbide Berkovich tip (Synton-MDP, Nidau, Switzerland) was used for all experiments. The frame stiffness and area function of the tip were obtained by indentation tests on a reference sample of fused quartz at RT according to the analysis of Oliver and Pharr [24]. To ensure correct contact temperatures a tip temperature calibration was performed by direct indentation into a thermocouple, as suggested by Wheeler and Michler [32]. Tip and sample are heated independently and carefully adjusted to stabilize the correct isothermal contact temperature. To follow any possible degradation of the indentation tip, after every tested sample indentations were performed on fused quartz. Also

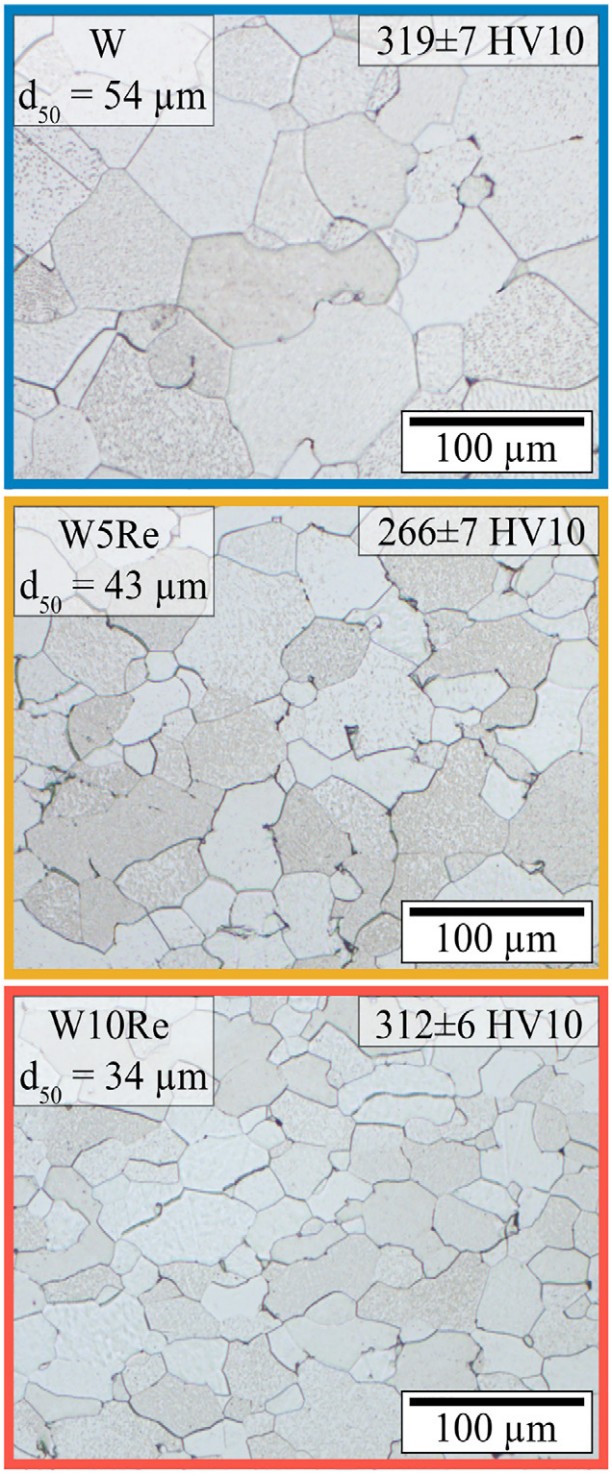

Fig. 1. Light optical micrographs of the investigated coarse-grained materials. The grain boundaries were contrasted with a Murakami etching. Vickers hardness HV10 and mean grain sizes are indicated in the according image.

after high-temperature testing the samples surfaces were examined in a light optical microscope to exclude any surface oxidation.

Nanoindentation experiments were conducted from RT (25 °C) up to 800 °C with temperature increments of 100 °C. To acquire Young's modulus E and hardness H, experiments with a constant indentation strain rate [33] $\dot{\varepsilon} = 0.5\dot{P}/P = 0.2\ s^{-1}$ up to a maximum indentation depth of 600 nm or to maximum load (50 mN) were performed. Hardness and Young's modulus at each temperature were averaged between indentation depths of 300 and 450 nm.

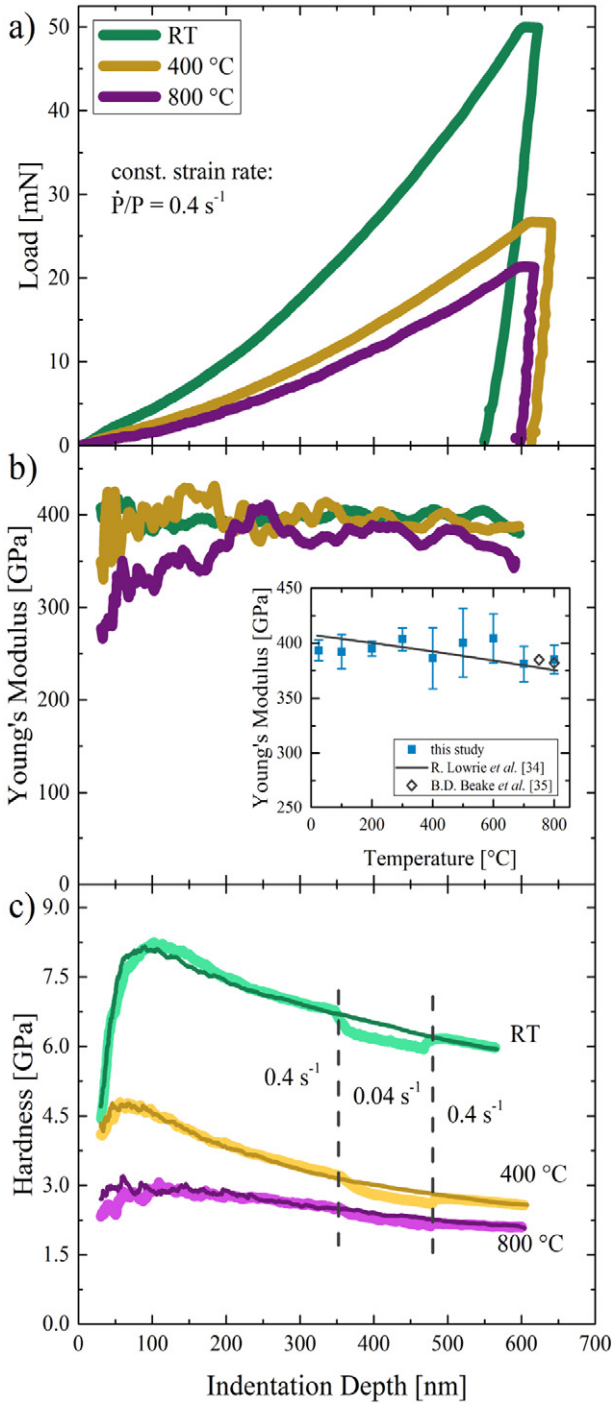

Fig. 2. Representative indentation data for W at RT, 400 °C and 800 °C: a) Load displacement curves, b) Young's modulus and c) hardness plotted overindentation depth for tests with constant indentation strain rate. The inset in b) shows the Young's modulus over temperature for technically pure W. In c) additional curves for strain rate jump tests are presented.

To obtain strain rate sensitivity $m = \partial(\ln(H))/\partial(\ln(\dot{\varepsilon}))$ and activation volume $V^* = C^* \cdot \sqrt{3} \cdot k_B \cdot T/(m \cdot H)$ of the materials, additional strain rate jump tests were performed, as introduced by Maier et al. [27], where C^* is a constraint factor taken as 2.8. Up to 350 nm the indentation strain rate was kept constant at $\dot{P}/P = 0.4\ s^{-1}$, followed by an abrupt rate change to $\dot{P}/P = 0.04\ s^{-1}$ for 125 nm and finally going back to the initial $\dot{P}/P = 0.4\ s^{-1}$ for another 125 nm. At least six valid indents were performed for every indentation protocol, material, as well as temperature.

3. Results

Comparing the Vickers hardness values for the three investigated materials in Fig. 1 indicates a pronounced solid solution softening effect. While W and W10Re exhibit almost identical values of 319 ± 7 and 312 ± 6 HV10, W5Re is significantly softer (266 ± 7 HV10). This is clearly linked to a change in the intrinsic material behavior, as for the continuously decreasing grain size from 54 μm (W) to 34 μm (W10Re) an increase in hardness according to Hall-Petch would be expected.

Fig. 2 shows representative indentation data for W at RT, 400 °C and 800 °C. The top (a) and center (b) indicate load and Young's modulus versus displacement for constant indentation strain rate tests. In the inset of Fig. 2b Young's modulus for W is shown as a function of temperature with additional literature values [34, 35]. The continuously recorded constant Young's modulus over indentation depth, as well as the accordance of our data with literature emphasize the accuracy of this data even at high temperatures. Finally, in Fig. 2c hardness over displacement is displayed for both testing protocols, constant indentation strain rate as well as strain rate jump tests. As expected for coarse-grained materials a decrease in hardness with increasing indentation depth, a so-called indentation size effect [36], can be observed, but was not investigated in detail, as the main focus of this study is on thermally activated deformation processes.

The measured hardness as a function of the homologous temperature T/T_m for the three tested materials is illustrated in Fig. 3. T_m for W is 3695 K, while the solidus temperature for W5Re and W10Re strongly decreases to 3493 K and 3418 K, respectively [37].

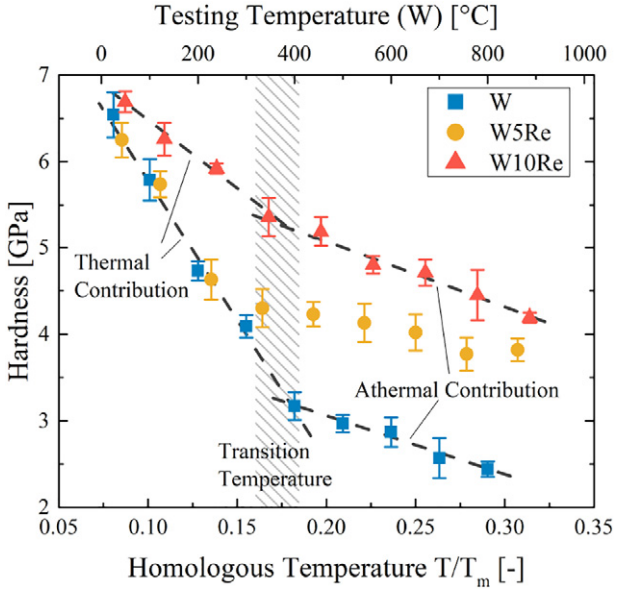

Fig. 3. Evolution of hardness over homologous temperature T/T_m for the three investigated materials at constant indentation strain rates. Thermal and athermal contribution to hardness are highlighted for W and W10Re. The transition temperature between these two regimes is well pronounced around 0.2 T_m.

The evolution of hardness over temperature is qualitatively similar for all three materials. From ambient to medium temperatures (~400 °C) we observe a rapid decrease in hardness, followed by a less temperature-sensitive, athermal part at higher temperatures. The transition temperature between these two different behaviors is slightly below 0.2 T_m. With increasing Re-content the level of athermal hardness is increased, while the slope of the thermal part or temperature-sensitivity $\partial H/\partial(T/T_m)$ is decreased. Solid solution softening is evident at RT hardness values of 6.54, 6.25 and 6.69 GPa for W, W5Re and W10Re and can be observed for W5Re for 100 °C and 200 °C as well. Overcoming 300°C the effect reverses and solid solution hardening takes place.

Strain rate sensitivity, activation volume and activation energy are plotted as a function of temperature in Fig. 4. For the strain rate sensitivity (Fig. 4a) of W we observe an increase from 0.021 at RT to a peak of 0.037 at 300 °C, followed by a steady decrease with increasing temperature. Alloying with Re lowers the strain rate sensitivity and no significant increase from ambient to medium temperatures can be observed. Overcoming approximately 400 °C all three alloys show a steady decrease over temperature. The activation volume, normalized to the cubed Burgers vector b of W (0.274 nm), in Fig. 4b generally increases with rising temperature. Starting from a value of $8b^3$ for W at RT, it increases to above $200b^3$ at 800 °C. The alloyed variants show a slightly higher activation volume below 400 °C. This effect disappears at temperatures exceeding 500 °C, where the activation volume is found independent of the alloy composition. From the hardness and Young's modulus data the apparent activation energy Q can be ascertained using the modulus-compensated hot hardness analysis [38, 39] $H/E = G' \cdot exp(Q \cdot m/(R \cdot T))$, where G' is a pre-exponential factor and R the gas constant. m-values are averaged in the associated temperature regime. This is summarized in Fig. 4c, where the data can be well described by linear fits in two different temperature regimes.

4. Discussion

A typical evolution of hardness over temperature for *bcc* metals with a pronounced thermal and athermal contribution to the flow stress [4, 5] can be observed in Fig. 3a. The athermal hardness values for W amounting to 40% of the RT hardness as well as a transition temperature around 400 °C are in excellent agreement with literature data [29, 40, 41]. Below 0.2 T_m alloying with Re manifests as a reduced temperature-sensitivity $\partial H/\partial(T/T_m)$. In the athermal deformation regime an increase in hardness for the alloyed materials can be observed, as is usually the case for solid solution strengthening [4]. The increase in athermal contribution on the one hand and the decrease in temperature sensitivity of the thermal contribution on the other hand leads to a solid solution softening for W5Re at RT up to 200 °C.

Fig. 4a shows a pronounced rate-sensitivity for W at RT, which is typical for *bcc* metals [4, 9, 42]. An increase in strain rate sensitivity can be observed up to 300 °C, followed by a steady decrease at higher temperatures. It is assumed that the initial increase below 0.2 T_m, which is common for 'technically pure' or doped *bcc* metals, stems from a thermally activated interaction of kinks with impurity atoms [5, 42-44]. The decrease of strain rate sensitivity at temperatures above 0.2 T_m results from thermal activation of dislocation movement via kinks [9]. As alloying with Re increases the athermal hardness, it generally decreases the strain rate sensitivity. This behavior is commonly observed during solid solution softening in refractory metals [19, 45] and is closely related to the reduced temperature sensitivity in the temperature regime below 0.2 T_m. Notably, the strain rate sensitivity for W5Re remains constant, or even increases slightly between RT and 100 °C. It can be assumed that, as for the technically pure W, thermally activated interaction of dislocations with impurity

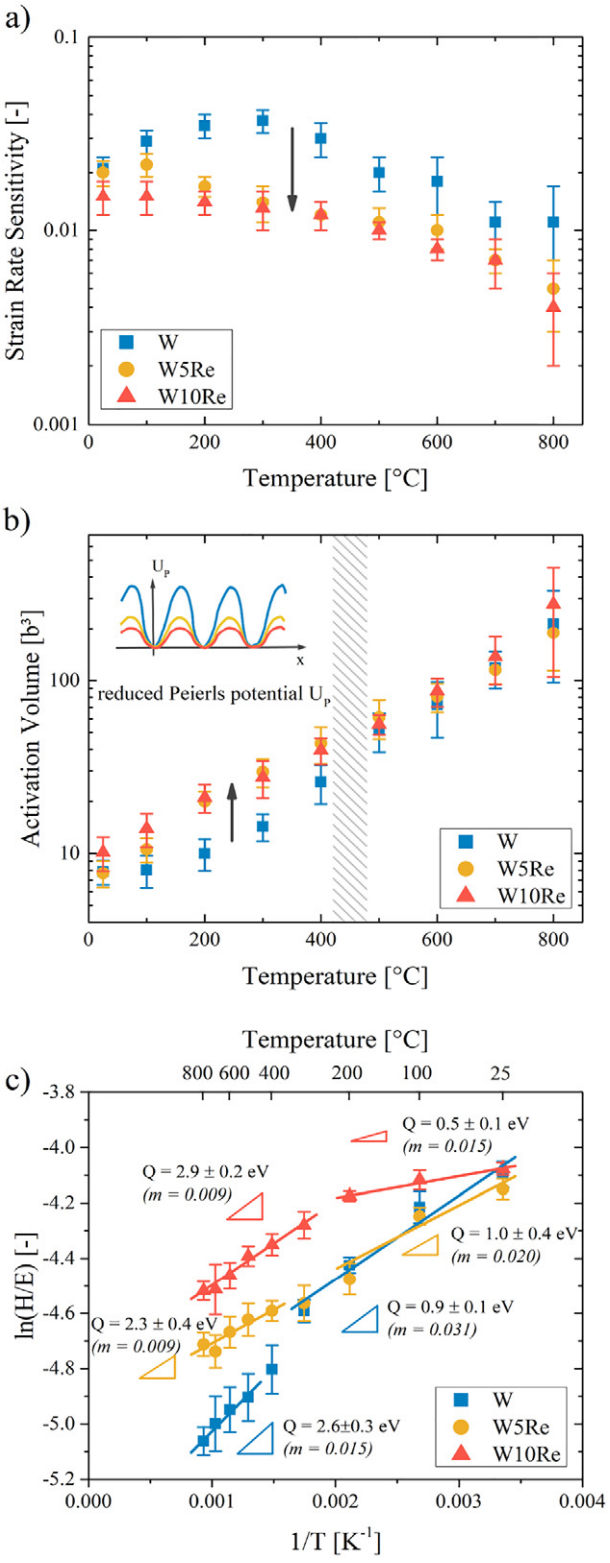

Fig. 4. Strain rate sensitivity a), activation volume b) and activation energy c) as a function of temperature. In a) the arrow indicates the reduced strain rate sensitivity due to alloying with Re, while in b) the arrow highlights the increased activation volume as a result of the reduced Peierls potential. The temperature regime, where the activation volume is independent of the Re content (above 400 °C) is emphasized as well. c) shows how activation energies of plastic deformation are determined with the modulus-compensated hot hardness analysis for two different temperature regimes.

atoms governs this effect. This behavior diminishes at higher temperatures due to the dominating effect of the substitutional Re atoms in the W lattice, a phenomenon that is described as 'scavenging' of interstitial impurities by solute atoms [46].

The activation volume describes the atoms collectively involved in the rate limiting deformation process [25] and is an indicator for the dominant plastic deformation mechanism. A value of around $10b^3$ at RT (Fig. 4b) points to a kink-pair mechanism [7], which is dominant at ambient temperatures for *bcc* metals in general [4, 9, 43]. At temperatures below 500 °C, the activation volume is significantly increased for the alloyed materials. This is related to a reduction in the Peierls potential due to the reorganization of the screw dislocation core by Re and the resulting increase in mobility, as reported in [6, 19]. Increasing the temperature to above 500 °C raises the activation volume to values larger than $100b^3$. This indicates that the deformation mechanism changes to dislocation-dislocation interaction via forest hardening, a more *fcc*-like behavior [5,42,43,47]. It should be noted that there is no change in the activation volume of the technically pure W between RT and 100 °C A conceivable explanation for that could be that impurity atoms hinder the thermal activation of kinks in that temperature regime. This assumption is supported by a similar observation for single crystal Cr [43, 47]. At testing temperatures of 500 °C and above, corresponding to 0.2 T_m for all three materials, the activation volume is independent of the Re content. As expected, this suggests that the rate limiting dislocation interaction in the athermal deformation regime is not strongly affected by the alloying element.

The activation energy at low temperatures is significantly reduced for W10Re (0.5 ± 0.1 eV), while 0.9 ± 0.1 eV for W is close to the activation energy of kink-pair formation at the critical resolved shear stress between 127 and 227 °C (1.11 eV) [48], although others found slightly higher values [49, 50]. In references [47] and [49] it is assumed that kink-pair formation below 0.2 T_m can be subdivided into a line-tension and elastic interaction dominated regime. One could presume a similar behavior in the W-data in Fig. 4 from the small bend at 200 °C. To verify such a transient, narrower temperature increments would be necessary. In the present study, values are averaged over the whole thermally activated deformation regime, as the main focus lies on the temperature regime exceeding 0.2 T_m, where only limited data can be found in literature. Here, No significant influence of Re (2.6 ± 0.3 eV, 2.3 ± 0.4 eV and 2.9 ± 0.2 eV for W, W5Re and W10Re, respectively) on the activation energy was confirmed.

5. Conclusion

Advanced high temperature nanoindentation methods were applied to study thermally activated deformation mechanisms in binary W-Re alloys. For that purpose three different coarse-grained alloys, namely commercially pure W, W5Re and W10Re were tested.

A reduction of the Peierls potential in W due to Re alloying was manifested as an increased activation volume of plastic deformation below 0.2 T_m. This results in a significantly decreased strain rate sensitivity and temperature dependency for the alloyed material variants. While the hardness in the athermal temperature regime was increased through conventional solid solution strengthening, the temperature-sensitivity in the thermal regime was drastically reduced. These two oppositional influences lead to the occurrence of solid solution softening in W5Re up to 200 °C.

To the authors' knowledge this is the first study that focuses on the plastic deformation behavior of W-Re alloys at temperatures significantly above the transition temperature from thermal to athermal flow stress. While solid solution softening can in some conditions be observed at low temperatures, at typical forming or application temperatures the mechanical behavior is governed by dislocation-dislocation interaction and a solution strengthening effect.

CRediT authorship contribution statement

Johann Kappacher: Formal analysis, Data curation, Visualization, Writing - original draft, Writing - review & editing. **Alexander Leitner:** Data curation, Validation. **Daniel Kiener:** Conceptualization, Validation, Writing - review & editing. **Helmut Clemens:** Validation, Resources, Writing - review & editing. **Verena Maier-Kiener:** Supervision, Conceptualization, Validation, Writing - review & editing.

Declaration of competing interest

The authors declare that they have no known competing financial interests or personal relationships that could have appeared to influence the work reported in this paper.

Acknowledgments

The authors want to thank Plansee SE for providing the material. D.K. acknowledges funding by the European Research Council under grant number 771146 (TOUGHIT).

References

[1] S. Oghi, On the coarsening of non-sag tungsten lamp filament wires, J. Phys. Soc. Jpn. 11 (5) (1956) 593–598. https://doi.org/10.1143/JPSJ.11.593.
[2] T. Palacios, J. Reiser, J. Hoffmann, M. Rieth, A. Hoffmann, J. Pastor, Microstructural and mechanical characterization of annealed tungsten (W) and potassium-doped tungsten foils, Int. J. Refract. Met. H. 48 (2015) 145–149. https://doi.org/10.1016/j.ijrmhm.2014.09.005.
[3] I. Šmid, H. Pacher, G. Vieider, U. Mszanowski, Y. Igitkhanov, G. Janeschitz, J. Schlosser, L. Plöchl, Lifetime of Be-, CFC-and W-armoured ITER divertor plates, J. Nucl. Mater. 233 (1996) 701–707. https://doi.org/10.1016/S0022-3115(96)00309-1.
[4] A. Argon, Strengthening Mechanisms in Crystal Plasticity, 4. Oxford University Press, New York. 2008.
[5] A. Seeger, The temperature and strain-rate dependence of the flow stress of body-centred cubic metals: a theory based on Kink-Kink interactions, Z. Metallkd. 72 (6) (1981) 369–380.
[6] L. Romaner, C. Ambrosch-Draxl, R. Pippan, Effect of rhenium on the dislocation core structure in tungsten, Phys. Rev. Let. 104 (19) (2010) 195503. https://doi.org/10.1103/PhysRevLett.104.195503.
[7] B. Sestak, A. Seeger, Gleitung und verfestigung in kubisch-raumzentrierten Metallen und Legierungen, Z. Metallkd. 69 (4) (1978) 195–202.
[8] B.G. Butler, J.D. Paramore, J.P. Ligda, C. Ren, Z.Z. Fang, S.C. Middlemas, K.J. Hemker, Mechanisms of deformation and ductility in tungsten-a review, Int. J. Refract. Met. H. 75 (2018) 248–261. https://doi.org/10.1016/j.ijrmhm.2018.04.021.
[9] V. Maier, A. Hohenwarter, R. Pippan, D. Kiener, Thermally activated deformation processes in body-centered cubic Cr-how microstructure influences strain-rate sensitivity, Scripta Mater. 106 (2015) 42–45. https://doi.org/10.1016/j.scriptamat.2015.05.001.
[10] G. Geach, J. Hughes, Plansee Proceedings, Plansee Proc. XXII (1956) 245–253.
[11] W.D. Klopp, Review of ductilizing of group VIA elements by rhenium and other solutes, NASA TN D-4955 (1968).
[12] H. Gao, R. Zee, Effects of rhenium on creep resistance in tungsten alloys, J. Mater. Sci. Lett. 20 (10) (2001) 885–887. https://doi.org/10.1023/A:1010915012522.
[13] A. Elsas, T. Zimmer, Höhere Belastung von Drehanodenröhren durch Verwendung von legierten Anoden, Rofo. Fortschr. Rontg. 97 (10) (1962) 511–514.
[14] H. Bolt, V. Barabash, W. Krauss, J. Linke, R. Neu, S. Suzuki, N. Yoshida, A.U. Team, Materials for the plasma-facing components of fusion reactors, J. Nucl. Mater. 329 (2004) 66–73. https://doi.org/10.1016/j.jnucmat.2004.04.005.
[15] T. Tanno, M. Fukuda, S. Nogami, A. Hasegawa, Microstructure development in neutron irradiated tungsten alloys, Mater. Trans. (2011) 1447–1451. https://doi.org/10.2320/matertrans.MBW201025.
[16] J. Webb, S. Gollapudi, I. Charit, An overview of creep in tungsten and its alloys, Int. J. Refract. Met. H. (2019) https://doi.org/10.1016/j.ijrmhm.2019.03.022.
[17] C.E. Beck, S.G. Roberts, P.D. Edmondson, D.E. Armstrong, Effect of alloy composition & helium ion-irradiation on the mechanical properties of tungsten, tungsten-tantalum & tungsten-rhenium for fusion power applications, MRS Online Proc. Libr. Arch. 1514 (2013) 99–104. https://doi.org/10.1557/opl.2013.356.

[18] A. Xu, C. Beck, D.E. Armstrong, K. Rajan, G.D. Smith, P.A. Bagot, S.G. Roberts, Ion-irradiation-induced clustering in W-Re and W-Re-Os alloys: a comparative study using atom probe tomography and nanoindentation measurements, Acta Mater. 87 (2015) 121–127. https://doi.org/10.1016/j.actamat.2014.12.049.
[19] P.L. Raffo, Yielding and fracture in tungsten and tungsten-rhenium alloys, J. Less-Common Metals 17 (2) (1969) 133–149. https://doi.org/10.1016/0022-5088(69)90047-2.
[20] Y. Zhao, J. Marian, Direct prediction of the solute softening-to-hardening transition in W-Re alloys using stochastic simulations of screw dislocation motion, Model. Simul. Mater. Sc. 26 (4) (2018) 045002. https://doi.org/10.1088/1361-651X/aaaecf.
[21] J.R. Stephens, W.R. Witzke, Alloy softening in group VIA metals alloyed with rhenium, J. Less-Common Metals 23 (4) (1971) 325–342. https://doi.org/10.1016/0022-5088(71)90043-9.
[22] A. Luo, D. Jacobson, K. Shin, Solution softening mechanism of iridium and rhenium in tungsten at room temperature, Int. J. Refract. Met. H. 10 (2) (1991) 107–114. https://doi.org/10.1016/0263-4368(91)90028-M.
[23] Y.-J. Hu, M.R. Fellinger, B.G. Butler, Y. Wang, K.A. Darling, L.J. Kecskes, D.R. Trinkle, Z.-K. Liu, Solute-induced solid-solution softening and hardening in bcc tungsten, Acta Mater. 141 (2017) 304–316. https://doi.org/10.1016/j.actamat.2017.09.019.
[24] W.C. Oliver, G.M. Pharr, An improved technique for determining hardness and elastic modulus using load and displacement sensing indentation experiments, J. Mater. Res. 7 (6) (1992) 1564–1583. https://doi.org/10.1557/JMR.1992.1564.
[25] V. Maier-Kiener, K. Durst, Advanced nanoindentation testing for studying strain-rate sensitivity and activation volume, J. Mater. Res. 69 (11) (2017) 2246–2255. https://doi.org/10.1007/s11837-017-2536-y.
[26] R. Schwaiger, B. Moser, M. Dao, N. Chollacoop, S. Suresh, Some critical experiments on the strain-rate sensitivity of nanocrystalline nickel, Acta Mater. 51 (17) (2003) 5159–5172. https://doi.org/10.1016/S1359-6454(03)00365-3.
[27] V. Maier, K. Durst, J. Mueller, B. Backes, H.W. Höppel, M. Göken, Nanoindentation strain-rate jump tests for determining the local strain-rate sensitivity in nanocrystalline Ni and ultrafine-grained Al, J. Mater. Res. 26 (11) (2011) 1421–1430. https://doi.org/10.1557/jmr.2011.156.
[28] J. Wheeler, D. Armstrong, W. Heinz, R. Schwaiger, High temperature nanoindentation: the state of the art and future challenges, Curr. Opin. Solid St. M. 19 (6) (2015) 354–366. https://doi.org/10.1016/j.cossms.2015.02.002.
[29] A.J. Harris, B.D. Beake, D.E. Armstrong, M.I. Davies, Development of high temperature nanoindentation methodology and its application in the nanoindentation of polycrystalline tungsten in vacuum to 950 C, Exp. Mech. 57 (7) (2017) 1115–1126. https://doi.org/10.1007/s11340-016-0209-3.
[30] B.D. Beake, A.J. Harris, Nanomechanics to 1000 C for high temperature mechanical properties of bulk materials and hard coatings, Vacuum 159 (2019) 17–28. https://doi.org/10.1016/j.vacuum.2018.10.011.
[31] J.S.-L. Gibson, S. Schröders, C. Zehnder, S. Korte-Kerzel, On extracting mechanical properties from nanoindentation at temperatures up to 1000 C, Extreme Mech. Lett. 17 (2017) 43–49. https://doi.org/10.1016/j.eml.2017.09.007.
[32] J. Wheeler, J. Michler, Elevated temperature, nano-mechanical testing in situ in the scanning electron microscope, Rev. Sci. Instrum. 84 (4) (2013) 045103. https://doi.org/10.1063/1.4795829.
[33] B. Lucas, W. Oliver, Indentation power-law creep of high-purity indium, Metall. Mater. Trans. A 30 (3) (1999) 601–610. https://doi.org/10.1007/s11661-999-0051-7.
[34] R. Lowrie, A. Gonas, Dynamic elastic properties of polycrystalline tungsten, 24-1800 C, J. Appl. Phys. 36 (7) (1965) 2189–2192. https://doi.org/10.1063/1.1714447.
[35] B.D. Beake, A.J. Harris, J. Moghal, D.E. Armstrong, Temperature dependence of strain rate sensitivity, indentation size effects and pile-up in polycrystalline tungsten from 25 to 950 C, Mater. Des. 156 (2018) 278–286. https://doi.org/10.1016/j.matdes.2018.06.063.
[36] W.D. Nix, H. Gao, Indentation size effects in crystalline materials: a law for strain gradient plasticity, J. Mech. Phys. Solids 46 (3) (1998) 411–425. https://doi.org/10.1016/S0022-5096(97)00086-0.
[37] E. Savitskii, M. Tylkina, S. Ipatova, E. Pavlova, Properties of tungsten-rhenium alloys, Met. Sci. Heat Treat. 2 (9) (1960) 483–486.
[38] O. Renk, V. Maier-Kiener, I. Issa, J. Li, D. Kiener, R. Pippan, Anneal hardening and elevated temperature strain rate sensitivity of nanostructured metals: their relation to intergranular dislocation accommodation, Acta Mater. 165 (2019) 409–419. https://doi.org/10.1016/j.actamat.2018.12.002.
[39] O. Sherby, P. Armstrong, Prediction of activation energies for creep and self-diffusion from hot hardness data, Metall. Mater. Trans. B 2 (12) (1971) 3479–3484. https://doi.org/10.1007/BF02811630.
[40] J.S.-L. Gibson, S.G. Roberts, D.E. Armstrong, High temperature indentation of helium-implanted tungsten, Mat. Sci. Eng. A 625 (2015) 380–384. https://doi.org/10.1016/j.msea.2014.12.034.
[41] X. Xiao, D. Terentyev, A. Ruiz, A. Zinovev, A. Bakaev, E.E. Zhurkin, High temperature nano-indentation of tungsten: modelling and experimental validation, Mat. Sci. Eng. A 743 (2019) 106–113. https://doi.org/10.1016/j.msea.2018.11.079.
[42] D. Brunner, V. Glebovsky, Analysis of flow-stress measurements of high-purity tungsten single crystals, Mater. Lett. 44 (3-4) (2000) 144–152. https://doi.org/10.1016/S0167-577X(00)00017-3.
[43] D. Kiener, R. Fritz, M. Alfreider, A. Leitner, R. Pippan, V. Maier-Kiener, Rate limiting deformation mechanisms of bcc metals in confined volumes, Acta Mater. 166 (2019) 687–701. https://doi.org/10.1016/j.actamat.2019.01.020.
[44] J.W. Christian, B. Masters, Low-temperature deformation of body-centred cubic metals I. Yield and flow stress measurements, Proc. Royal Soc. Lond. A 281 (1385) (1964) 223–239. https://doi.org/10.1098/rspa.1964.0180.
[45] S. Nemat-Nasser, R. Kapoor, Deformation behavior of tantalum and a tantalum tungsten alloy, Int. J. Plasticity 17 (10) (2001) 1351–1366. https://doi.org/10.1016/S0749-6419(00)00088-7.
[46] K. Ravi, R. Gibala, The strength of niobium-oxygen solid solutions, Acta Metall. Mater. 18 (6) (1970) 623–634. https://doi.org/10.1016/0001-6160(70)90091-X.
[47] I.-C. Choi, C. Brandl, R. Schwaiger, Thermally activated dislocation plasticity in body-centered cubic chromium studied by high-temperature nanoindentation, Acta Mater. 140 (2017) 107–115. https://doi.org/10.1016/j.actamat.2017.08.026.
[48] A. Giannattasio, S.G. Roberts, Strain-rate dependence of the brittle-to-ductile transition temperature in tungsten, Philos. Mag. 87 (17) (2007) 2589–2598. https://doi.org/10.1080/14786430701253197.
[49] D. Brunner, Comparison of flow-stress measurements on high-purity tungsten single crystals with the kink-pair theory, Mater. T. JIM 41 (1) (2000) 152–160. https://doi.org/10.2320/matertrans1989.41.152.
[50] L. Dezerald, L. Proville, L. Ventelon, F. Willaime, D. Rodney, First-principles prediction of kink-pair activation enthalpy on screw dislocations in bcc transition metals: V, Nb, Ta, Mo, W, and Fe, Phys. Rev. B 91 (9) (2015) 094105. https://doi.org/10.1103/PhysRevB.91.094105.